Acta Pharmacologica Sinica

ARTICLE

Ainsliadimer C, a disesquiterpenoid isolated from *Ainsliaea macrocephala*, ameliorates inflammatory responses in adipose tissue via Sirtuin 1-NLRP3 inflammasome axis

Cheng Chen[1], Yong-mei Ren[2], Jian-zhong Zhu[1], Jia-li Chen[1], Zhe-ling Feng[1], Tian Zhang[1], Yang Ye[2] and Li-gen Lin[1]

Interleukin-1β (IL-1β), a key pro-inflammatory cytokine, is majorly produced by macrophages through NOD-, LRR-, and pyrin domain-containing protein 3 (NLRP3) inflammasome, which has been identified as the culprit to deteriorate the inflammatory crosstalk between macrophages and adipocytes. Ainsliadimer C (AC) is a disesquiterpenoid isolated from *Ainsliaea macrocephala*. In the current study, we investigated the effects of AC on adipose tissue inflammation in co-culture of macrophages and adipocytes in vitro as well as in LPS-treated mice in vivo. We showed that AC (20–80 μM) dose-dependently inhibited the secretion of IL-1β from LPS plus ATP-stimulated THP-1 macrophages by inhibiting the activation of NLRP3 inflammasome. Furthermore, we found that AC treatment activated NAD^+-dependent deacetylase Sirtuin 1 (SIRT1), resulting in reduced acetylation level of NLRP3. Molecular modeling analysis revealed that binding of AC to sirtuin-activating compound-binding domain increased the affinity of the substrate to the catalytic domain of SIRT1. Moreover, AC (80 μM) significantly attenuated macrophage-conditioned medium-induced inflammatory responses in 3T3-L1 adipocytes. In LPS-induced acute inflammatory mice, administration of AC (20, 60 $mg{\cdot}kg^{-1}{\cdot}d^{-1}$, ip) for 5 days significantly suppressed the pro-inflammatory cytokine levels in serum and epididymal white adipose tissue (eWAT), attenuated macrophage infiltration into eWAT, and mitigated adipose tissue inflammation. The beneficial effects of AC were blocked by co-administration of a selective SIRT1 inhibitor EX-527 (10 $mg{\cdot}kg^{-1}{\cdot}d^{-1}$). Taken together, AC suppresses NLRP3-mediated IL-1β secretion through activating SIRT1, leading to attenuated inflammation in macrophages and adipose tissue, which might be a candidate to treat obesity-associated metabolic diseases.

Keywords: Ainsliadimer C; interleukin-1β; macrophages; NLRP3 inflammasome; Sirtuin 1; adipose tissue inflammation; obesity; metabolic disorders; EX-527; dexamethasone

Acta Pharmacologica Sinica (2022) 43:1780–1792; https://doi.org/10.1038/s41401-021-00797-z

INTRODUCTION

Long-term low-grade inflammation is a determining factor in the onset and development of obesity-associated metabolic disorders [1]. Growing evidence suggests that abdominal fat is the major source of inflammatory mediators [2]. In adipose tissue from lean objects, the resident immune cells secrete pro- and anti-inflammatory cytokines, and maintain insulin sensitivity [3]. However, in obese objects, more monocytes infiltrate into adipose tissue and differentiate into pro-inflammatory macrophages, which produce pro-inflammatory cytokines, including tumor necrosis factor-α (TNF-α), interleukin-1β (IL-1β), IL-6, and monocyte chemoattractant protein 1 (MCP-1), causing adipose tissue inflammation and insulin resistance [4, 5]. Inflammation is mainly triggered in adipose tissue, and then chronic inflammation of adipose tissue causes systemic inflammation in other metabolic organs [6]. Therefore, therapeutic interventions targeting adipose tissue macrophages (ATMs) have attracted widespread attention in prevention and treatment of metabolic disorders.

NOD-, LRR-, and pyrin domain-containing protein 3 (NLRP3) inflammasome, coupled with the adaptor apoptosis-associated speck-like protein containing a carboxy-terminal caspase-recruitment domain (ASC) and pro-caspase 1, triggers the mutation of caspase 1, resulting in the cleavage of the cytokine precursor pro-IL-1β to release the mature IL-1β [3]. IL-1β is a key pro-inflammatory cytokine majorly secreted by macrophages and monocytes, which impairs insulin sensitivity and induces the expression and secretion of pro-inflammatory factors in human adipocytes [5, 7]. Suppressing IL-1β activity attenuates adipose tissue inflammation in obese mice [8]. Therefore, suppression of NLRP3-caspase 1 pathway and subsequent IL-1β production in macrophages is essential in alleviating adipose tissue inflammation. Recent study has shown that acetylation of NLRP3 is crucial for its activation [9]. Sirtuin 1 (SIRT1), a nicotinamide adenine dinucleotide$^+$ (NAD^+)-dependent protein deacetylase, has been considered as a promising target in alleviating inflammation [10, 11].

[1]State Key Laboratory of Quality Research in Chinese Medicine, Institute of Chinese Medical Sciences, University of Macau, Macao 999078, China and [2]State Key Laboratory of Drug Research and Natural Products Chemistry Department, Shanghai Institute of Materia Medica, Chinese Academy of Sciences, Shanghai 201203, China
Correspondence: Yang Ye (yye@simm.ac.cn) or Li-gen Lin (ligenl@um.edu.mo)
These authors contributed equally: Cheng Chen, Yong-mei Ren, Jian-zhong Zhu, Jia-li Chen.

Received: 20 June 2021 Accepted: 13 October 2021
Published online: 17 November 2021

The plants of *Ainsliaea* genus (Compositae family) are mainly distributed in Southeast Asia and widely used as folk medicines to treat various diseases, such as fever, cold, rheumatism, pharyngitis, and trauma [12]. Sesquiterpenoids are the major constituents of the plants of *Ainsliaea* genus, which have been reported with anti-inflammatory properties. Ainsliadimer A is a potent inhibitor of nuclear factor-κB (NF-κB) [13]. Our previous study found that macrocephadiolides A and B, isolated from *A. macrocephala*, showed anti-inflammatory effect on lipopolysaccharide (LPS)-treated RAW264.7 macrophages [14]. Ainsliadimer C (AC, Fig. 1a) is a disesquiterpenoid isolated from *A. macrocephala* [15], possessing a purity of 94.44% and 98.83% via a diode array detector and an evaporative light scattering detector, respectively (Supplementary Fig. S1). Herein, the effects of AC against adipose tissue inflammation on the co-culture of macrophages and adipocytes and LPS-treated mice, as well as the underlying mechanisms, were investigated.

MATERIALS AND METHODS

Ethic

The procedures and operations involved in the animal experiments were conducted under the Animal Ethical and Welfare Committee of University of Macau (No. ICMS-AEC-2014–06) regulation and conformed to the ARRIVE guidelines. The male C57BL/6J mice were maintained in the animal facility of Faculty of Health Science, University of Macau. The mice were fed with normal chow diet (18% protein, 4.5% fat, and 58% carbohydrate, Guangdong Medical Lab Animal Center, Guangzhou, China) and water *ad libitum* under standard conditions (specific-pathogen-free) with air filtration (22 ± 2 °C, 12-h light/12-h dark).

Animal experimental procedure

According to the body weight, 33 male mice (6-week-old) were randomly separated into seven groups ($n = 3$–5). The vehicle and LPS + ATP groups of mice were intraperitoneally injected with 10 mL/kg polyethylene glycol 400 (PEG 400, Sigma-Aldrich, St. Louis, MO, USA) solution (PEG 400:0.9% saline, 6:4, *v/v*). The remaining five groups of mice were intraperitoneally injected with 20 mg/kg AC (AC-L, 2 mg/mL AC in PEG 400 solution), 60 mg/kg AC (AC-H, 6 mg/mL AC in PEG 400 solution), 10 mg/kg selisistat (Sigma-Aldrich, EX-527, 1 mg/mL, dissolved with PEG 400 solution under shaking at room temperature), the combination of 10 mg/kg EX-527 and 60 mg/kg AC (AC + EX-527, 1 mg/mL EX-527 and 6 mg/mL AC in PEG 400 solution), and 4 mg/kg dexamethasone (Sigma-Aldrich, DEX, 0.4 mg/mL dexamethasone in PEG 400 solution), respectively, once a day for consecutive 5 days. On the sixth day, the vehicle group of mice was intraperitoneally injected with 10 mL/kg phosphate buffer saline (PBS). The other six groups of mice were administered with 4 mg/kg LPS (Sigma-Aldrich, serotype O111:B4, 0.4 mg/mL LPS in PBS) and after 4 h followed by 30 mg/kg ATP (Sigma-Aldrich, 3 mg/mL ATP in PBS, pH 6.2) by peritoneal injection. 0.5 h after ATP injection, blood samples were collected from tail vein under anesthesia (0.5 L/min inhalation of 3% isoflurane). The mice were euthanized by deeply inhaling carbon dioxide, and peritoneal macrophages and epididymal white adipose tissue (eWAT) were collected and stored at −80 °C.

Cell culture

Human THP-1 cells and murine 3T3-L1 preadipocytes were obtained from American Type Culture Collection (Manassas, VA, USA). THP-1 cells (passage number 15–30) were maintained in RPMI-1640 (Gibco, Gaithersburg, MD, USA) supplemented with 10% heat-inactivated fetal bovine serum (FBS, Gibco). To differentiate into macrophages, THP-1 cells were cultured with phorbol 12-myristate polymerized 13-ester ester (PMA, 100 ng/mL, Sigma-Aldrich) for 12 h. Peritoneal macrophages were isolated from 12-week-old C57BL/6J mice. After sacrificed, the mice were intraperitoneally injected with 5 mL PBS and shaken for 3 min. Subsequently, the PBS was aspirated and centrifuged at 400 × *g* for 5 min. The cell pellet was collected and incubated in RPMI-1640 supplemented with 10% FBS and P/S (100 units/mL of penicillin and 100 μg/mL of streptomycin, Thermo-Fisher, Grand Island, NY, USA). After 1 week, the nonadherent cells were removed and the adherent cells were kept for further experiments.

3T3-L1 preadipocytes (passage number 15–25) were maintained in Dulbecco's modified Eagle's medium (DMEM) containing 10% calf serum (Gibco) and P/S. 3T3-L1 cells were differentiated into adipocytes as reported previously [4]. Two days post confluent, 3T3-L1 preadipocytes were cultured in DMEM supplemented with 10% FBS, 1 μM DEX, 0.5 mM 3-isobutyl-1-methylxanthine (IBMX, Sigma-Aldrich), and 5 μg/mL insulin (Sigma-Aldrich) for 2 days. Subsequently, cells were cultured in maintenance medium (DMEM supplemented with 10% FBS and 5 μg/mL insulin, changed every other day) for 6 days. The differentiation of 3T3-L1 cells was confirmed by microscopic observation and Oil-Red O staining. A representative image of Oil-Red O staining is shown in Supplementary Fig. S2.

Cell viability

Cell viability was evaluated by 3-(4,5-dimethylthiazol-2-yl)−2,5-diphenyltetrazolium bromide (MTT, Sigma-Aldrich) assay [16]. Macrophages were seeded into 96-well plates at a density of 1×10^4 cells per well. After adherence, macrophages were treated with compounds for 24 h. Then macrophages were cultured in DMEM containing MTT (1 mg/mL) for 4 h, and finally 100 μL DMSO was used to dissolve the formazan crystals attached to the bottom of well. The absorbance at 570 nm was measured by a SpectraMax M5 microplate reader (Molecular Devices, San Jose, CA, USA).

Co-culture of macrophages and adipocytes

Macrophage-adipocyte co-culture was performed as described previously [4]. THP-1 macrophages were treated with or without 80 μM AC for 12 h, and then stimulated with LPS (1 μg/mL) for 4 h and then 1 mM ATP for 1 h. After washing twice with RPMI-1640 medium, THP-1 macrophages were incubated in fresh RPMI-1640 medium for 24 h. The macrophage supernatant was collected as macrophage conditioned medium (CM). The fully differentiated 3T3-L1 adipocytes were incubated with CM for 24 h. The content of nitric oxide (NO) in the supernatant was determined with Griess reagent (Sigma-Aldrich) [4, 17].

Harvest protein from cell culture medium

THP-1 cell culture medium was collected and centrifuged at 15,000 × *g* for 10 min at 4 °C. Supernatant (700 μL) were transferred to a new tube and mixed thoroughly with 700 μL methanol and 175 μL chloroform. After standing at room temperature for 5 min, the mixture was centrifuged, and the white intermediate layer was collected. After washed with methanol, the protein sample in culture medium was dissolved in SDS sample buffer for Western blotting analysis.

Cytokines levels

The ELISA kits (Neobioscience, Shenzhen, China) were used to determine the cytokine levels in cell culture medium, mouse serum, and adipose tissue lysates, according to the instructions.

Western blotting analysis

Western blotting was performed as described previously [18]. THP-1 macrophages, mouse-derived peritoneal macrophages, and eWAT were fully lysed with RIPA lysis buffer (Beyotime, Shanghai, China). The protein concentration was determined by the BCA Protein Assay Kit (Thermo-Fisher). The same amount of protein was separated by SDS-PAGE and transferred to the PVDF membrane (Bio-Rad, Hercules, CA, USA). The membranes were blocked with 5% non-fatty milk in TBST buffer (100 mM NaCl, 10 mM Tris-HCl, pH 7.5, and 0.1% Tween-20) for 1 h at room temperature, and incubated with specific primary antibodies (Supplementary Table S1) overnight at 4 °C. After incubating the

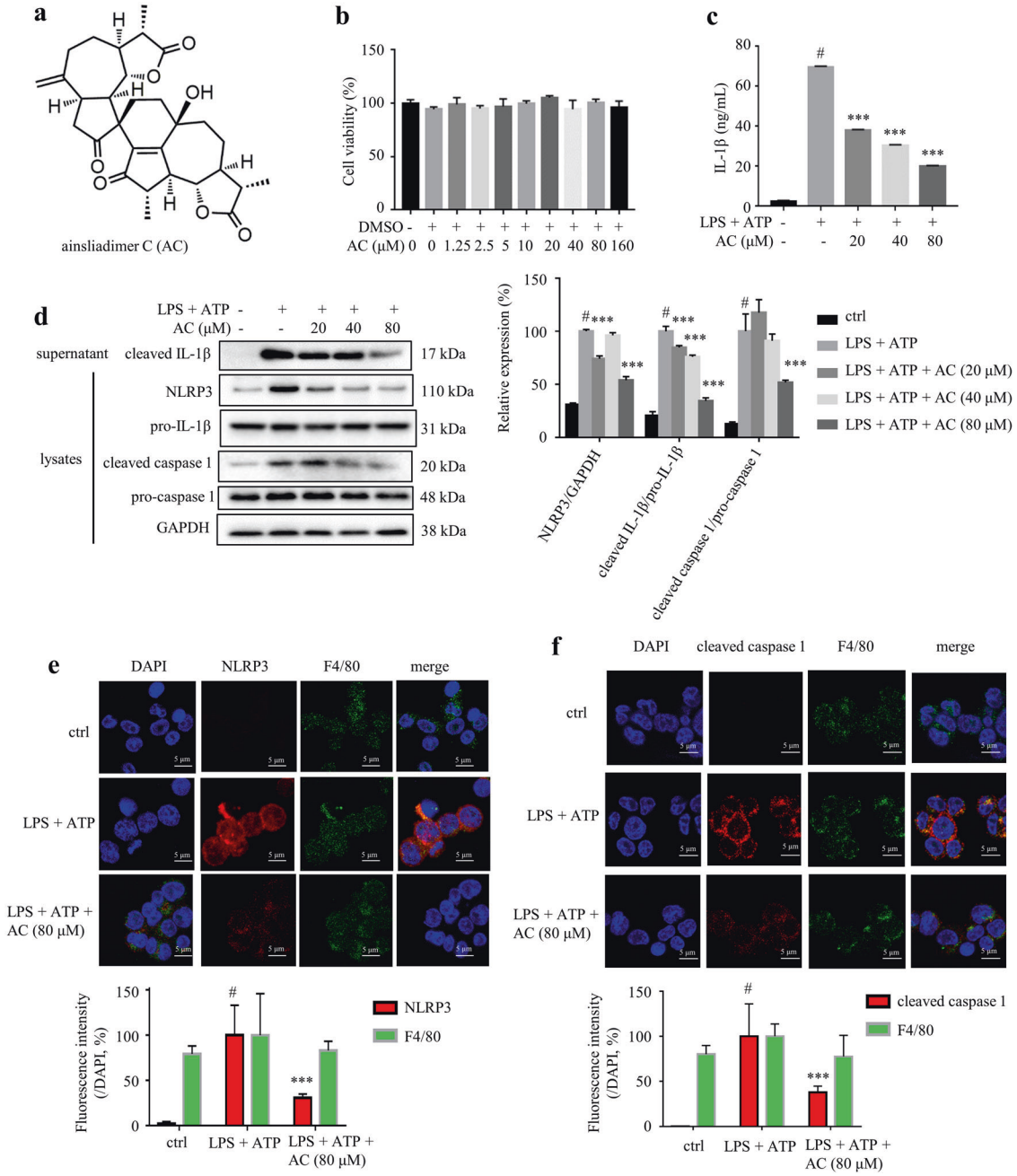

Fig. 1 AC suppressed LPS plus ATP-stimulated IL-1β secretion in THP-1 cells. a Chemical structure of AC. **b** Cytotoxicity of AC on THP-1 cells assessed by MTT assay. THP-1 cells were treated with different concentrations of AC (from 1.25 to 160 μM) for 24 h ($n = 6$). **c** The levels of IL-1β in the culture medium from THP-1 cells ($n = 3$). THP-1 cells were cultured in the presence or absence of AC for 12 h, and stimulated with LPS for 4 h and then ATP for 1 h. **d** The expression of NLRP3, pro-caspase 1, cleaved caspase 1, pro-IL-1β in the lysates, and cleaved IL-1β in the supernatant of THP-1 cells detected by Western blotting. GAPDH was chosen as an internal loading control ($n = 5$). Immunofluorescence staining of NLRP3 (**e**) and cleaved caspase 1 (**f**) ($n = 3$). Scale bar = 10 μm. Data are expressed as means ± SEM. $^{\#}P < 0.05$ versus DMSO, $^{***}P < 0.001$ versus LPS + ATP.

horseradish peroxidase-conjugated secondary antibody for 1 h at room temperature, specific protein bands were analyzed using SuperSignal West Femto Maximum Sensitivity Substrate (Thermo-Fisher), visualized using the ChemiDoc MP Imaging System (Bio-Rad), and quantitated using Image Lab 5.1 [19].

Computer modeling

Molecular docking was performed on AutoDock 4.2 (The Scripps Research Institute, La Jolla, CA, USA). The crystal structure of the quaternary complex (PDB ID: 4ZZJ) [20] was employed as the receptor. The protein was firstly prepared at pH 7.4 with all the water molecules removed and corresponding hydrogen atoms added. The 3D structure of AC was converted from the 2D structure drawn on ChemDraw 19.0 (PerkinElmer, Waltham, MA, USA) and then manually checked for its conformation. Gasteiger charge was assigned, and a 19.5 Å × 20.25 Å × 21 Å grid box with a grid spacing of 0.375 Å was placed to include the shallow hydrophobic small molecule sirtuin-activating compound (STAC)

binding domain (SBD). The genetic algorithm was chosen for docking calculations, and 50 genetic algorithm runs were performed. The acquired poses were clustered with a tolerance of 2.0 Å.

All molecular dynamics simulations were carried out on the Gromacs 2020.4 (KTH Royal Institute of Technology, Stockholm, Sweden) package using the amber14SB forcefield [21]. The initial structures of the complex were acquired from the docking results. The protonation status was determined on the PDB2PQR webserver (https://server.poissonboltzmann.org/pdb2pqr). All the ligands were parameterized according to the general amber forcefield [22] using the antechamber program of AmberTools 18, and the topology/coordinate files were acquired by parmchk2, tleap, and were further converted to Gromacs format using the *acpype* python script [23]. Temperature was maintained at 310 K by the V-rescale thermostat, and pressure was maintained at 1 bar by Parinello-Rahman barostat. Periodic boundary conditions were applied to the simulation system, the bond lengths involved in hydrogen atoms were constrained by the LINCS algorithm, and the equations of motion were integrated using the leap-frog scheme with a time step of 2 fs. The particle-mesh Ewald method was used to evaluate long-range electrostatic interactions; a cut off value of 1.2 nm was used for Van der Waals interaction and short-range electrostatic interactions. The system was solvated in TIP3P water and neutralized by adding Na^+ or Cl^-. After energy minimization and pre-equilibration (1 ns), production run was conducted.

Cellular thermal shift assay (CETSA)

THP-1 cells were treated with or without 80 μM AC for 12 h, and then fully lysed with RIPA lysis buffer. Cell lysates were adjusted to 2 μg/μL and heated for 5 min at different temperatures (50–90 °C). After cooling on ice, samples were collected by centrifugation at 12,000 × *g* for 20 min at 4 °C for Western blotting analysis [24, 25].

SIRT1 deacetylating activity

SIRT1 deacetylating activity was determined with a SIRT1 fluorometric assay kit (Sigma-Aldrich). Fluorescence intensity was detected at an excitation wavelength of 355 nm and an emission wavelength of 450 nm.

Immunoprecipitation

The indicated antibody was mixed with 20 μL protein A/G-Sepharose beads (Santa Cruz Biotechnology, Santa Cruz, CA, USA) and incubated at 4 °C for 4 h. Cell lysates were added and incubated overnight at 4 °C. After washed twice with PBS, lysis buffer and sample preparation buffer were added. Samples were boiled for 5 min and then used for Western blotting analysis.

Immunofluorescence staining

Immunofluorescence staining was performed as described previously [26]. THP-1 cells were fixed on glass coverslips pre-coated with collagen with 4% paraformaldehyde. Then the specific primary antibody (1:100 dilution) was added and incubated at 4 °C for 30 min. After washed twice with TBST buffer, the corresponding secondary antibody (1:1000 dilution) was added and incubated for 30 min at room temperature. A confocal microscope (Olympus, Tokyo, Japan) was used for detection of fluorescent images.

Histological analysis

The eWAT was fixed in 10% buffered formalin, and then embedded in paraffin. H&E staining was performed according to standard experimental procedures.

Immunohistochemistry

For immunohistochemistry, 6 μm deparaffinized sections of eWAT were eluted with different concentrations of xylene-ethanol eluent gradient. Sodium citrate antigen retrieval solution (Beyotime) was added for boiling twice, followed by incubating with anti-F4/80 (1:100 dilution, Santa Cruz Biotechnology) and anti-Perilipin-1 (1:100 dilution, Cell Signaling Technologies, MA, USA) antibodies overnight at 4 °C. The slides were incubated with the corresponding secondary antibodies for 2 h at room temperature.

Druggability analysis

The druggability analysis of AC was calculated by SwissADME, a tool provided by the Swiss Institute of Bioinformatics (Lausanne, Switzerland) [27]. Molecular weight, number of stereo crystal centers, number of hydrogen bond acceptors, number of hydrogen bond donors, number of rotatable bonds, number of rings, sp^3 carbon fraction, and aromatic heavy atom fraction of AC were calculated according to the website instruction [28], to predict absorption, distribution, metabolism, and excretion (ADME) parameters, pharmacokinetic properties, druglike nature, and medicinal chemistry friendliness of AC.

Statistical analysis

All experimental data were analyzed by the GraphPad Prism 8.0 (GraphPad software, San Diego, CA, USA) and presented as mean ± SEM. Student's *t*-test for comparisons between two groups and one-way analysis of variance for multiple comparisons were conducted to evaluate the significant differences. *P* value less than 0.05 was considered statistically significant.

RESULTS

AC suppressed LPS plus ATP-stimulated IL-1β secretion in THP-1 macrophages

Macrophage-secreted IL-1β plays a critical role in insulin resistance and pro-inflammatory response of adipocytes from obese subjects [7]. AC is a disesquiterpenoid isolated from the whole plants of *A. macrocephala* [14]. LPS plus ATP-induced inflammation model has been widely used in biological and pharmacological studies [5, 29]. There are two-step mechanisms for full activation of NLRP3 inflammasome. First, priming signal such as LPS recognizes Toll-like receptors and induces production of pro-IL-1β. Second, some cellular danger signals including ATP trigger K^+ efflux and pannexin-1 membrane pore formation, which are responsible for NLRP3 activation. Then, it activates casepase-1 to cleave pro-IL-1β to be its active form [30]. Herein, the inhibitory effect of AC on IL-1β secretion was tested on THP-1 macrophages stimulated by LPS plus ATP. AC was not cytotoxic to THP-1 macrophages up to 160 μM (Fig. 1b). ELISA results showed that AC dose-dependently inhibited the release of IL-1β in culture medium from LPS plus ATP-induced THP-1 cells (Fig. 1c). The NLRP3 inflammasome is the key regulator of the production of IL-1β in macrophages [31]. As expected, AC treatment inhibited the expression of NLRP3 and the cleavage of caspase 1 in the cell lysates, and the expression of cleaved IL-1β in the cell culture medium from THP-1 macrophages induced by LPS plus ATP, assessed by Western blots (Fig. 1d). The expression of the adaptor ASC was unchanged in AC-treated THP-1 cells (Supplementary Fig. S3). The immunofluorescence staining of NLRP3 and cleaved caspase 1 provided further support to the above observation (Fig. 1e, f). These results indicated that AC suppresses the secretion of IL-1β in LPS plus ATP-induced THP-1 macrophages by inhibiting the activation of NLRP3 inflammasome.

AC inhibited the activation of NLRP3 inflammasome through activating SIRT1

The acetylation of NLRP3 is a switch of its activation [9]. Consistent with the positive control DEX, AC decreased LPS plus ATP-induced increase of acetylated NLRP3 (Fig. 2a). SIRT1, an NAD^+-dependent protein deacetylase, is involved in the activation of NLRP3 inflammasome [32–34]. Interestingly, LPS plus ATP treatment significantly decreased the protein level of SIRT1 while AC treatment increased SIRT1 expression in a dose-dependent

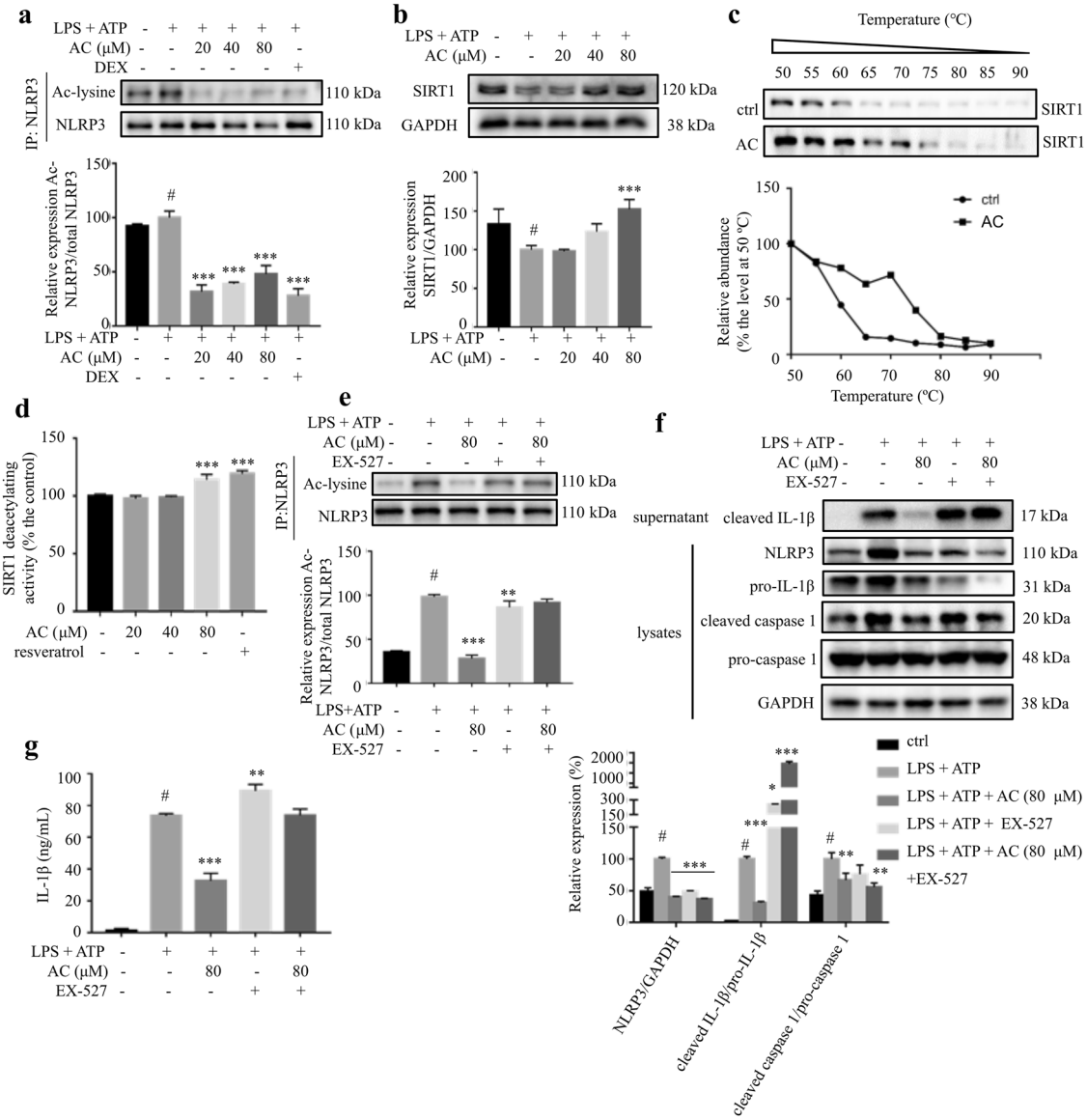

Fig. 2 AC inhibited the activation of NLRP3 inflammasome through activating SIRT1. THP-1 cells were treated with various concentrations of AC for 12 h, and then stimulated with LPS for 4 h and ATP for 1 h. **a** The acetylated and total NLRP3 protein levels ($n = 3$). **b** The expression level of SIRT1 detected by Western blotting ($n = 3$). GAPDH was chosen as an internal loading control. **c** CETSA performed on THP-1 cells after the treatment with or without AC (80 μM) for 12 h ($n = 3$). **d** The effect of AC or resveratrol on the deacetylating activity of SIRT1 ($n = 6$). The deacetylating activity was determined with a SIRT1 fluorometric assay kit. **e** The acetylated and total NLRP3 protein levels ($n = 3$). **f** The expression of NLRP3, pro-caspase 1, cleaved caspase 1, and pro-IL-1β in the lysates, and cleaved IL-1β in the supernatant of THP-1 cells detected by Western blotting ($n = 3$). GAPDH was chosen as an internal loading control. **g** The levels of IL-1β in the culture medium from THP-1 cells ($n = 6$). Data are expressed as means ± SEM. $^{\#}P < 0.05$ versus DMSO, $^{**}P < 0.01$, $^{***}P < 0.001$ versus LPS + ATP.

manner (Fig. 2b). CETSA was performed to explore whether AC interacts with SIRT1. Compared with the control cells, AC treatment obviously stabilized SIRT1 at various temperatures (Fig. 2c). Indeed, the SIRT1 fluorometric assay results indicated that AC improved the deacetylating activity of SIRT1, which was comparable with resveratrol, a known SIRT1 activator (Fig. 2d). EX-527, a highly potent and selective SIRT1 inhibitor (IC_{50} is 38 nM in a cell-free assay, exhibits >200-fold selectivity against SIRT2 and SIRT3) [35], effectively inhibited the deacetylating activity of SIRT1 (Supplementary Fig. S4), which was used to confirm the effect of AC. When co-treated with EX-527, the suppressing effects of AC on the acetylation level of NLRP3 and the expression of cleaved caspase 1 in lysates and cleaved IL-1β in supernatants were almost blocked (Fig. 2e, f). Furthermore, co-treatment withEX-527 totally reversed the suppressing effect of AC on IL-1β secretion in cell culture medium (Fig. 2g). These results suggested that the inhibitory effects of AC on IL-1β production and NLRP3 activation were mediated through activating SIRT1 deacetylase.

AC bound to the STAC binding domain to activate SIRT1

To investigate whether AC could bind to SIRT1, molecular docking was firstly performed to evaluate the binding possibility of AC to SIRT1. From the 50 runs, 14 conformations were predicted to bind at the same site with favorable energy (Fig. 3a). The best pose in the predominant cluster (the green bar, Fig. 3a) showed a score of −6.67 kCal/mol, and it packed over the shallow hydrophobic surface depression as previously described (Fig. 3b). Specifically, AC showed hydrophobic interaction with L206, T209, I210, P211, P212, L215, I223, and I227; and was hydrogen bonded with the nitrogen atom (2.6 Å) on the amide moiety from the sidechain of

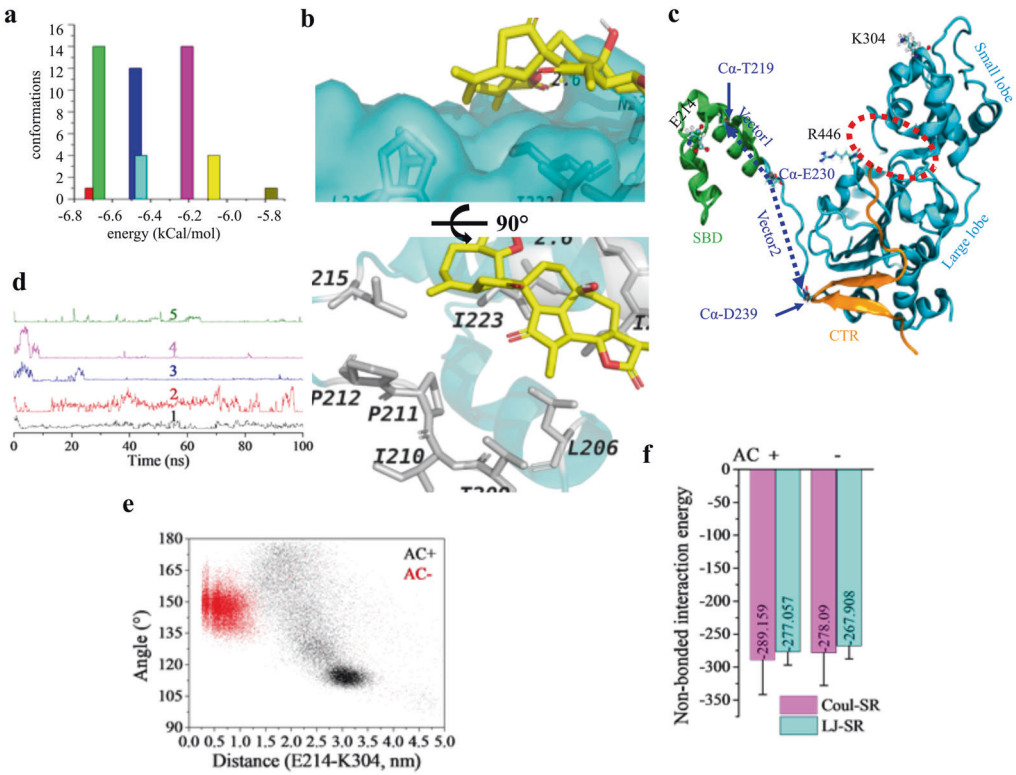

Fig. 3 AC is a potential activator of SIRT1. a Docking results of AC to the reported allosteric activation site of SIRT1 (PDB ID: 4ZZJ). Cluster analysis of the acquired conformations from AutoDock 4.2 using a tolerance of 2.0 Å. **b** Interactions between AC and residues on SIRT1 of the most possible binding conformation. Residues and AC are shown in white gray and yellow sticks. Hydrogen bond is indicated in yellow dashed line. **c** SIRT1 structure showing key domains, amino acid pairs, and the two vectors monitored. Protein structure was shown in NewCartoon, E214 and K304 were shown in CPK, and R446 was displayed as Licorice; the red dashed circle indicates the catalytic cleft; α-carbon atoms were shown in VDW; vector defined from the Cα of E230 to that of T219 was termed as vector1 and to that of D239 was termed as vector 2. **d** Changes of the distance as a function of time between the carboxyl oxygen atoms of E230 and the nitrogen atoms on the guanidyl group of R446 from five independent dynamic simulations in the holo structure. **e** Scatter plots showing the conformation distribution in the presence/absence of AC using the angle from the two vectors and the distance between E214 and K304. **f** Non-bonded interaction energy between the substrate and the catalytic domain calculated from the stable trajectories of the holo structure and that in state 2 of the apo structure. Coul-SR short-range Coulomb interaction energy, LJ-SR short-range Lennard–Jones potential.

N226 (yellow dashed line, Fig. 3b). This docking conformation further supported that AC increased the SIRT1 deacetylating activity.

To further explore the possible activation conformation, we firstly evaluated the probability that the key amino acid pair (E230 and R446, Fig. 3c) bind together from the initial open crystal conformation. Five independent dynamics simulations using the holo structure (with AC) were performed (Fig. 3d), where three trajectories showed very stable binding (blue, magenta, and green line) and one trajectory displayed fluctuated but still positive binding (black line). However, this binding trend was also observed in the apo structure without AC (Supplementary Fig. S5a). Two 1.2-μs long trajectories were accordingly produced to scrutinize the conformation difference. After about 700 ns, the substrate was stabilized in the holo structure (Supplementary Fig. S5b), whereas it seemed to flip between two states in the apo structure (Supplementary Fig. S6c). Interestingly, E230 and R446 got separated in the holo structure (Supplementary Fig. S6a, b). The distance between the amino acid residue pair (E214 and K304) and the angle defined by the two vectors (Fig. 3c) were monitored to differentiate the conformations of the SBD, and the scatter plot produced showed that SBD had greater mobility in the apo structure (Fig. 3e) with both the angle and the distance between E214 and K304 showing different probability distribution (Supplementary Fig. S6c, d). Despite being insignificant, AC enhanced the non-bonded interaction of the substrate to the catalytic domain (Fig. 3f) when compared to that in state 2 of the apo structure (Supplementary Fig. S5c). Although the non-bonded interaction between the substrate and the catalytic domain in state 1 was stronger than that in the holo structure (data not shown), state 1 was less stable and less frequent than state 2. Therefore, the binding of AC could in this way increase the affinity of the substrate to the catalytic domain, which could result in the observed enhancement in deacetylating activity of SIRT1.

The free energy landscape showed a very deep energy basin in the holo structure (Fig. 4a), whereas the protein flipped from one state to another by crossing an energy barrier (Fig. 4b). In the representative holo structure (Fig. 4c, d), extensive hydrophobic interaction network was found among the hydrophobic moiety on AC, the phenyl group on the substrate, and the residues (I215, I223, N226, and I227); N226 was additionally hydrogen bonded with AC and the substrate in a distance of 1.85 and 1.78 Å, respectively, whereas only hydrophobic interaction was seen between the phenyl group on the substrate and the residues (L206, I210, P211, and P212) on SBD in the representative conformation of basin 1 (cyan structure, Fig. 4e). Despite that N226 and S229 formed hydrogen bond with the substrate in the representative conformation of basin 2 (pink structure, Fig. 4e), it was less frequent as the conformations in basin 1.

AC attenuated macrophage-CM induced inflammatory responses in adipocytes

To evaluate the effect of macrophage-secreted cytokines on inflammatory responses in adipocytes, the fully differentiated 3T3-L1 adipocytes were treated with CM from THP-1 cells treated with

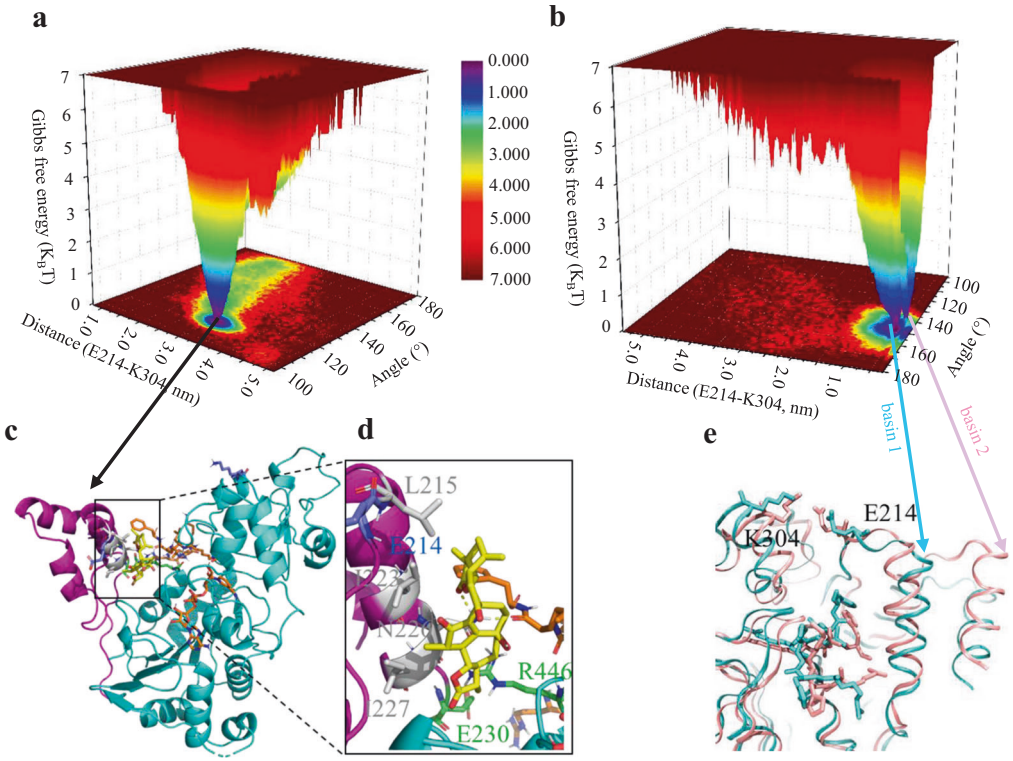

Fig. 4 Free energy landscape and representative conformations in the presence/absence of AC. a, **b** Free energy landscape of the holo structure and apo structure. Free energy surfaces are colored as gradient, where the units are expressed as K_BT. K_B is the Boltzmann constant and T isthe temperature. **c**–**e** Representative conformation in the energy basins of the holo structure and the apo structure. The SBD and catalytic domain were colored as magenta and cyan, respectively; residues, AC (yellow), NAD, and the substrate were shown in sticks; hydrogen bond was indicated as yellow dashed line.

AC or DMSO (Fig. 5a). Compared with the control group, the treatment with CM from LPS plus ATP-treated macrophages significantly increased the production of NO, IL-6, MCP-1, and TNF-α, which were significantly reversed by the treatment with CM from LPS plus ATP plus AC-treated macrophages (Fig. 5b–e). On the contrary, AC did not show anti-inflammatory effect on TNF-α-stimulated 3T3-L1 adipocytes (Supplementary Fig. S7). These results indicated that CM from AC-treated macrophages attenuated inflammatory responses in adipocytes.

AC treatment alleviated adipose tissue inflammation in LPS-stimulated mice

In order to further verify the anti-inflammatory effect of AC, an LPS plus ATP-induced acute inflammation mouse model was implemented (Fig. 6a). AC treatment showed no obvious effect on the body weight, indicating that AC was not toxic to mice (Fig. 6b). ELISA results showed an increase of IL-1β, IL-6, MCP-1, and TNF-α levels in serum from LPS plus ATP-treated mice, while pre-treatment with AC dose-dependently reversed this effect to an extent that was comparable to the positive control group (DEX) (Fig. 6c–f). These trends were partially blocked by the co-treatment with EX-527 (Fig. 6c–f). In addition, the levels of NLRP3, cleaved caspase 1, and cleaved IL-1β in the peritoneal macrophages from LPS and ATP-induced mice were suppressed by AC, which was reversed by the co-treatment with EX-527 (Fig. 6g). Therefore, AC mitigates LPS plus ATP-mediated inflammatory responses in mice probably through activating SIRT1.

Increased pro-inflammatory cytokines and elevated macrophages filtration are the main characteristics of adipose tissue inflammation. The infiltrated macrophages surround dead adipocytes to form crown-like structure, which is a typical characteristics of macrophage infiltration and adipose tissue inflammation. Herein, the H&E staining of eWAT sections from LPS and ATP-induced mice suggested more infiltration of macrophages when compared with the vehicle control, whereas the amount of macrophage infiltrated in eWAT was significantly curbed by AC treatment to a degree that was comparable with the DEX-treated mice (Fig. 7a). The immunohistofluorescent staining of F4/80, a macrophage marker, and perilipin-1, a major coating protein on the surface of lipid droplets to locate adipocytes, further supported the above observation (Fig. 7b). LPS and ATP-induced mice showed increased levels of F4/80 and CD68 in eWAT. However, this increase was significantly reduced in AC-treated mice (Fig. 7c). Similarly, the cytokine levels, including IL-1β, IL-6, MCP-1, and TNF-α, in eWAT from LPS and ATP-induced mice were elevated, which were significantly blocked by AC treatment (Fig. 7d–g). Interestingly, the co-treatment with EX-527 undermined the trends described above (Fig. 7a–g). These observations suggested that AC alleviates adipose tissue inflammation in LPS and ATP-induced mice by lessening macrophages infiltration.

DISCUSSION

Adipose tissue inflammation plays a key role in obesity- or aging-associated metabolic disorders [4, 36, 37]. The infiltration of macrophages and the expression of pro-inflammatory cytokines in adipose tissue promote chronic low-grade inflammation [38, 39]. ATMs are the main regulators that maintaining adipose tissue homeostasis and function in a healthy state by removing cell debris and absorbing lipids from adipocytes, while in a positive energy state, long-term over activation of ATM will lead to chronic low-grade inflammation [40]. From genetic obesity or diet-induced obese mice, pro-inflammatory cytokines in WAT are upregulated before the development of insulin resistance [41]. Many small molecules showed the potential to alleviate adipose tissue inflammation, resulting in salutary effects in metabolic

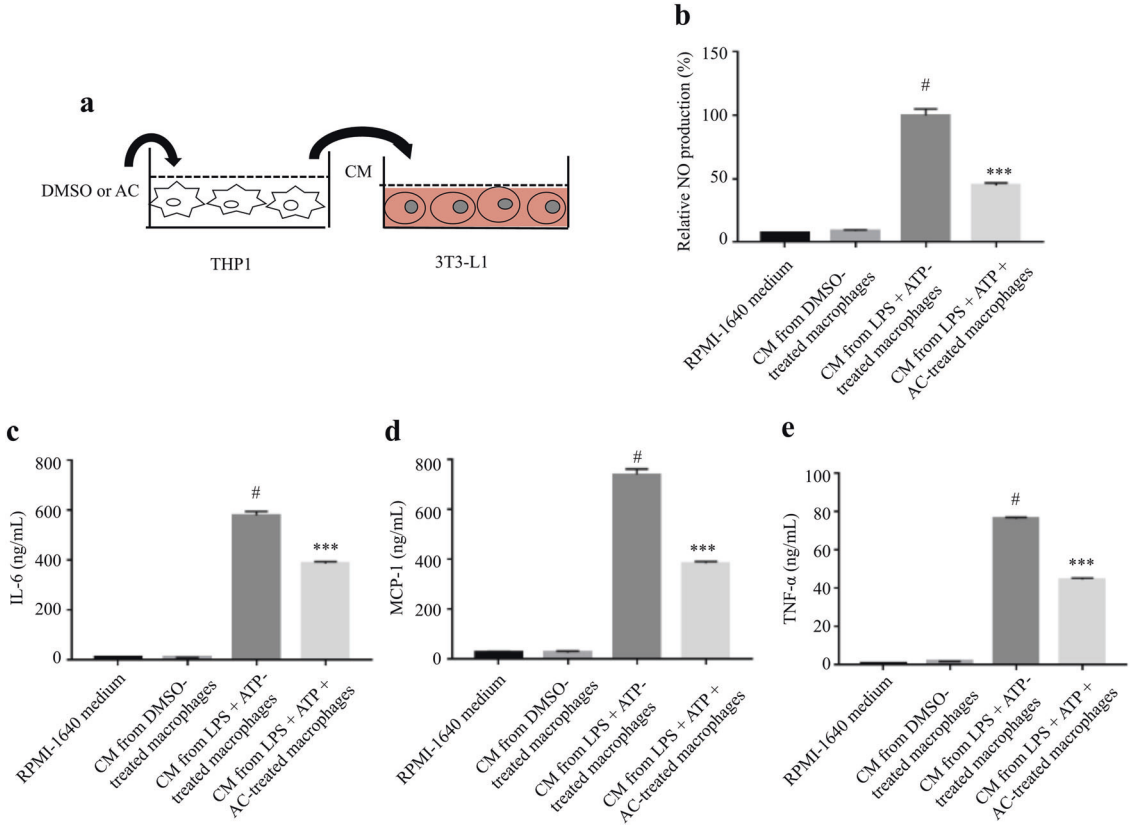

Fig. 5 AC attenuated macrophage-CM-induced inflammatory responses in adipocytes. a Schematic diagram of the experimental procedure. THP-1 cells were treated AC (80 μM) or DMSO for 12 h, and subsequently stimulated with LPS for 4 h and ATP (1 mM) for 1 h. After 24 h of culturing in fresh medium, the supernatants were collected as macrophage CM, which was used to incubate the fully differentiated 3T3-L1 for 24 h. The production of NO (**b**) and the levels of IL-6 (**c**), MCP-1 (**d**), and TNF-α (**e**) in 3T3-L1 adipocytes were determined. Data are expressed as means ± SEM. $n = 6$. $^{\#}P < 0.05$ versus DMSO, $^{***}P < 0.001$ versus LPS + ATP.

disorders [42]. Herein, AC was identified to alleviate inflammatory responses in LPS-stimulated macrophages and adipose tissue inflammation in LPS-induced mice, which represents a new scaffold to treat inflammation-associated metabolic diseases.

IL-1β is a pro-inflammatory cytokine secreted mainly by monocytes and macrophages, which is formed by cleavage of pro-IL-1β through NLRP3 inflammasome-mediated caspase 1 [43]. IL-1β is considered as the culprit to deteriorate the inflammatory crosstalk between macrophages and adipocytes [7]. IL-1β-mediated subclinical inflammation is involved in the formation of peripheral insulin resistance and high level of IL-1β has been found in the vitreous of diabetic retinopathy patient [44, 45]. LPS plus ATP promotes the production and secretion of IL-1β in macrophages, which in turn induces inflammation of adipocytes, leading to chronic low-grade inflammation. Since no ASC protein is expressed in RAW264.7 cells, mature NLRP3 inflammasome cannot be assembled to accomplish the cleavage of caspase 1 [46]. Alternatively, human-derived THP-1 macrophages were recruited in the current study. Our data showed that AC suppresses the production and release of IL-1β in THP-1 macrophages through suppressing the activation of NLRP3 inflammasome. In spite of this fact, we evaluated the anti-inflammation effect of AC on murine-derived RAW264.7 macrophages. The results indicated that AC dose-dependently decreased NO secretion through suppressing inducible NO synthase expression and NF-κB activation (Supplementary Fig. S8). In addition, we determined the expression of NLRP3, pro-caspase 1, cleaved caspase 1, pro-IL-1β in the lysates, and cleaved IL-1β in the supernatant of bone marrow-derived macrophages from mice. As expected, AC effectively curbed the increased levels of NLRP3, cleaved caspase 1, and cleaved IL-1β induced by LPS plus ATP in bone marrow-derived macrophages (Supplementary Fig. S9).

NLRP3 inflammasome is the central link in the development of metabolic diseases induced by metabolic danger signals [47–52]. The endogenous metabolic danger signals, such as amylin, cholesterol crystals, palmitate, ceramide, urate crystals, and amyloid β, activate the NLRP3 inflammasome, promote the secretion of IL-1β, and accelerate the progression of type 2 diabetes [47], atherosclerosis [48], non-alcoholic steatohepatitis [49], obesity [50], ulcerative colitis [53], and Alzheimer's disease [52]. Growing evidence indicates that suppressing the activation of NLRP3 inflammasome is beneficial to treat inflammation and metabolic disorders [54]. Ablation of NLRP3 prevented obesity-induced inflammation in mice fat depots [50]. The recent study indicated that acetylation of NLRP3 is essential for its activation [9]. Herein, AC suppressed NLRP3 inflammasome activation in both in vitro and in vivo models, which might be through reducing the acetylation of NLRP3.

SIRT1 is a member of the NAD^{+}-dependent deacetylases (SIRT1–7). SIRT1 catalyzes the deacetylation of histones and restores the dense state of chromatin, to downregulate the expression of many inflammation-related genes [55]. SIRT1 deacetylates the transcriptional factors NF-κB [56] and activator protein-1 [57] to suppress the expression of pro-inflammatory genes. SIRT1 decreases the acetylation level of sterol regulatory element-binding protein [58], to reduce its stability and DNA binding capacity, thereby inhibiting the activation of inflammasomes and the processing and secretion of IL-1β. Many studies have shown that SIRT1 shows anti-inflammatory effect through regulating the NLRP3 inflammasome [32, 33]. Our study showed

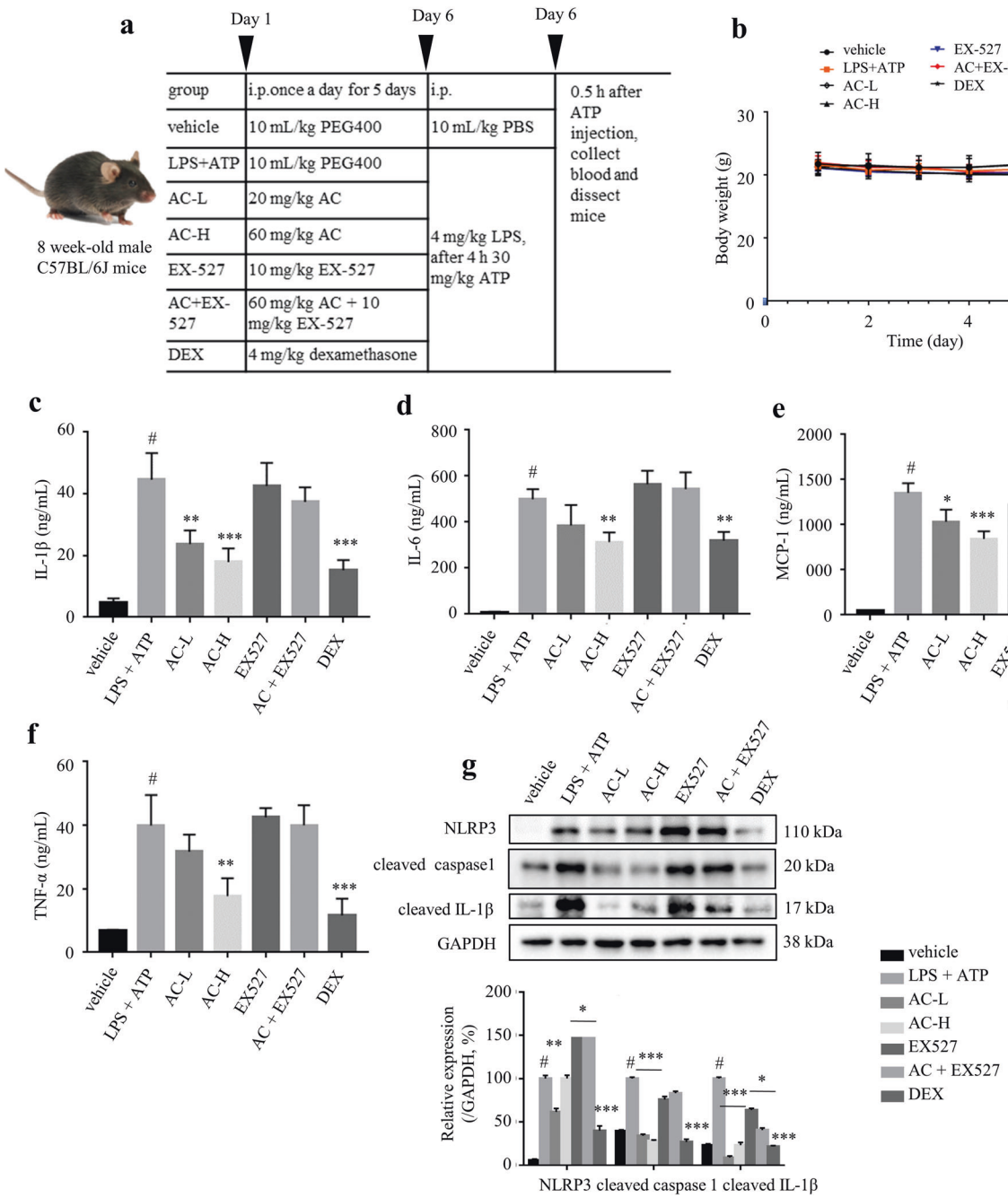

Fig. 6 AC treatment alleviated LPS plus ATP-mediated inflammatory responses in mice. a The inducement of in vivo acute inflammation model using LPS plus ATP. DEX: 4 mg/kg DEX; AC-L: 20 mg/kg AC; AC-H: 60 mg/kg AC; EX-527: 10 mg/kg EX-527; AC + EX-527: 60 mg/kg AC and 10 mg/kg EX-527. $n = 3–5$. **b** Changes of body weight. The serum levels of IL-1β (**c**), IL-6 (**d**), MCP-1 (**e**), and TNF-α (**f**). **g** NLRP3, cleaved IL-1β, and cleaved caspase 1 levels in peritoneal macrophages were analyzed by Western blotting. GAPDH was chosen as an internal loading control. Data are expressed as means ± SEM. $^{\#}P < 0.05$ LPS + ATP vs. vehicle; $^{*}P < 0.05$, $^{**}P < 0.01$, $^{***}P < 0.001$ AC-L, AC-H or DEX vs. LPS + ATP.

that AC increases the expression of SIRT1 and its deacetylating activity in THP-1 cells. It has been reported that SIRT2 directly interacts with NLRP3 [9]. When co-IP NLRP3, no SIRT1 protein was pulled down, suggesting no direct interaction between SIRT1 and NLPR3 (Supplementary Fig. S10). Thus, SIRT1 indirectly regulates the acetylation level of NLRP3, further studies are needed to uncover the regulatory loop. SIRT1 activators might be promising therapeutic agents to treat adipose tissue inflammation-related diseases.

A quaternary crystal structure (a STAC, NAD^{+} analog, a p53-derived substrate, and a mini-hSIRT1) was determined earlier, where the STAC bound to the shallow hydrophobic surface of SBD [20]. The interaction mode acquired from docking analysis in this study agreed well with the described interaction in this complex, suggesting the potential of AC to activate SIRT1 by binding to the SBD. It was suggested that E230 could form salt bridge with R446 dynamically, promoting the binding between the activator (or SBD) and the catalytic cleft [20]. Another salt bridge (between E214 and K304) was also indicated to be crucial in the activated binding conformation [59]. In this study, E230 and R446 bound together regardless of the presence of AC. However, the binding of AC resulted in a less motile conformation and enhanced the

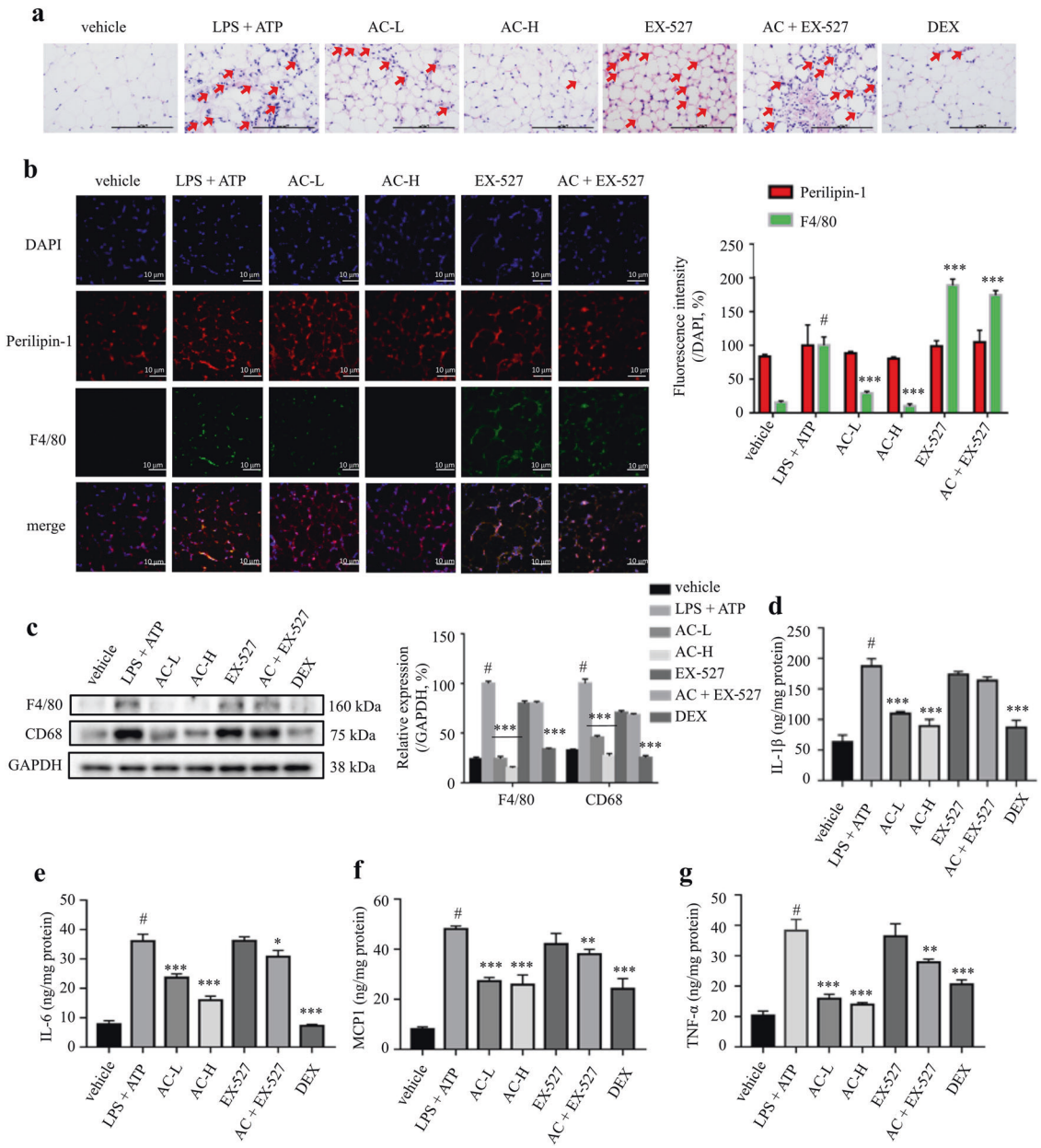

Fig. 7 AC treatment attenuated adipose tissue inflammation. a H&E staining of eWAT sections. Red arrows indicate the infiltrated macrophages in eWAT. Scale bar = 100 μm. **b** Immunofluorescence staining of perilipin-1 (red, marker of adipocytes) and F4/80 (green, marker of macrophages) in eWAT. Scale bar = 10 μm. **c** Expression levels of F4/80 and CD68 determined by western blotting. GAPDH was chosen as an internal loading control. The levels of IL-1β (**d**), IL-6 (**e**), MCP-1 (**f**), and TNF-α (**g**) in eWAT determined by ELISA. DEX: 4 mg/kg DEX; AC-L: 20 mg/kg AC; AC-H: 60 mg/kg AC; EX-527: 10 mg/kg EX-527; AC + EX-527: 60 mg/kg AC and 10 mg/kg EX-527. Data are expressed as means ± SEM (n = 3–5). $^{\#}P < 0.05$ LPS + ATP vs. vehicle; $^{*}P < 0.05$, $^{**}P < 0.01$, $^{***}P < 0.001$ AC-L, AC-H or DEX vs. LPS + ATP.

interaction between the substrate and the catalytic domain when compared to that in the more probable conformation in the apo structure. Interestingly, the distance between E214 and K304 was never close as previously reported [59]. The size of AC, in comparison to resveratrol, and the substrate with a different structure could be the reasons for this difference. The activation mechanism through SBD of SIRT1 remains to be elusive. Therefore, apart from partially supporting the notion that AC is an activator of SIRT1, we hope the stable binding conformation with AC in our in silico study here can help gain some insights into the activation mechanism of STACs in the scientific community. The binding pattern and specificity of AC on SIRT1 deacetylase are still unclear.

Dexamethasone is a glucocorticoid that prevents the release of inflammatory substances in the body, which has been widely used to treat many different inflammatory conditions such as allergic disorders, skin conditions, ulcerative colitis, and psoriasis [60]. Unfortunately, dexamethasone shows many side effects including diabetes, peptic ulcer, and Cushing's syndrome [61]. Thus, a lot of efforts have been paid to discover non-steroidal anti-inflammatory drug. AC is a disesquiterpenoid isolated from *A. macrocephala*, a widely used folk medicine to treat fever, cold, rheumatism, pharyngitis, and trauma. Hitherto, shot-term AC treatment did not show any adverse effect. Further toxicological studies are needed to fully verify its safety. Not like dexamethasone directly targeting glucocorticoid receptor, AC activates the deacetylase SIRT1 to exert its anti-inflammatory effect. SIRT1 modulates the initial and development of inflammation through deacetylating histones and critical transcription factor, thus leading to transcriptional

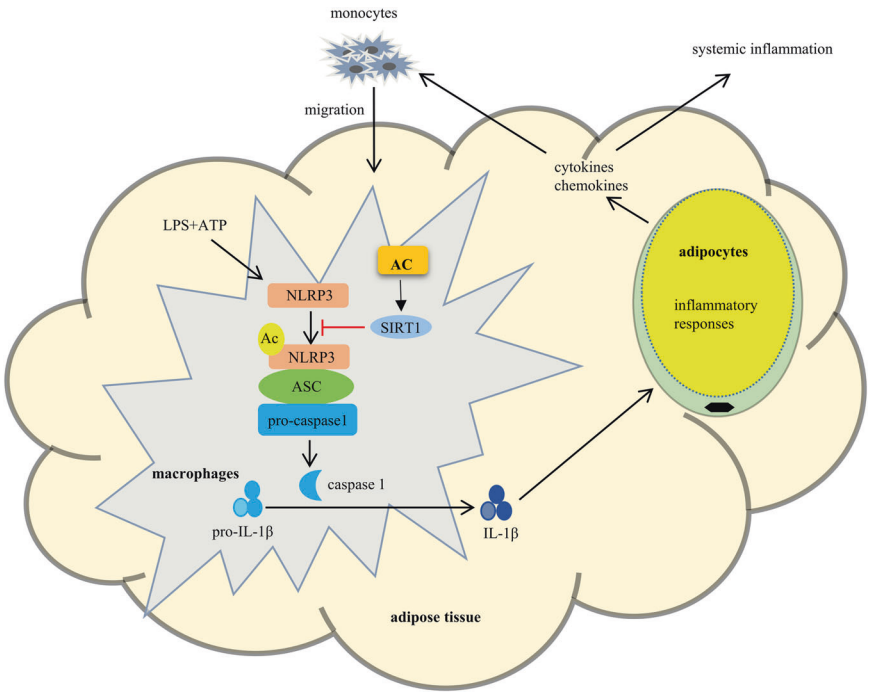

Fig. 8 Schematic model of AC in attenuating adipose tissue inflammation. Therapeutically, AC activates SIRT1 to suppress the activation of NLRP3 inflammasome, which in turn alleviates macrophages and adipose tissue inflammation by reducing the secretion of IL-1β.

repression of various inflammation-related genes, which is a promising therapeutic strategy for inflammation-related diseases [62].

Many molecules from traditional Chinese medicines have been reported to attenuate adipose tissue inflammation in various models [63–65]. Berberine promotes the polarization toward anti-inflammatory macrophages to reduce inflammation in adipose tissue [63], and salvianolic acid B inhibits high-fat-diet-induced inflammation by activating the nuclear factor erythroid 2–related factor 2 pathway [64]. The plants of *Ainsliaea* genus are widely used as folk medicines to treat inflammatory diseases. Ainsliadimer A is a structural analog of AC isolated from *A. macrocephala*, which possesses promising anti-inflammatory activity [13]. Together with our previous [14] and current studies, it might indicate that guaianolide-type sesquiterpenoids are a type of novel scaffold with anti-inflammatory potential. To predict its druggability, the ADME, drug similarity, and drug chemistry friendliness of AC were analyzed (Supplementary Table S2). And the physicochemical properties, pharmacokinetics, topological polar surface area (TPSA), logarithmic (LOG) S and iLOGP, and bioavailability properties of AC were also listed (Supplementary Table S2). The Log *P* value (2.84) and Log *S* value (−4.55) of AC indicated low oral bioavailability and poor water solubility. AC has a molecular weight of 508.60 g/mol, molar refractive index of 134.49, and TPSA of 106.97 $Å^2$. AC matches all Lipinski's rules except the molecular weight. The brain or intestinal estimated permeation method (BOILED-Egg) is proposed as an accurate predictive model that can predict the passive gastrointestinal (GI) absorption and brain entry of small molecules [66]. AC shows good GI absorption potential but poor ability to penetrate the blood–brain barrier. AC cannot inhibit any one of the five major isoforms of cytochrome P450 (CYP450), including CYP1A2, CYP2C19, CYP2C9, CYP2D6, and CYP3A4. Compared to the drugs from the FDA databases, AC has high drug similarity with eplerenone (0.954). Used for the treatment of chronic heart failure and high blood pressure, eplerenone is an aldosterone antagonist type of potassium-sparing diureti, particularly for patients with resistant hypertension caused by elevated aldosterone. Thus, AC might possess antihypertensive effect. Thus, AC has potential to be developed as a drug candidate. However, further structural optimization is needed to enhance its bioactivity and improve solubility and bioavailability.

In conclusion, AC, a sesquiterpenoid from *A. macrocephala*, inhibits the production and secretion of IL-1β in macrophages through the inactivation of NLRP3 inflammasome by SIRT1-mediated deacetylation (Fig. 8). AC blocks the inflammatory crosstalk between macrophages and adipocytes, and prevents the migration of macrophages into adipose tissue (Fig. 8). AC might be a drug candidate for the treatment of adipose tissue inflammation and related metabolic abnormalities.

ACKNOWLEDGEMENTS

This research was support by National Natural Science Foundation of China (81872754), the Science and Technology Commission of Shanghai Municipality (20430780300, 19431908100), the Science and Technology Development Fund, Macao SAR, China (File No. FDCT 0031/2019/A1), and the Research Fund of University of Macau (MYRG2018–00037-ICMS). The high-performance computing center ofUniversity of Macau is appreciated for providing computing services.

AUTHOR CONTRIBUTIONS

CC, YMR, JZZ, JLC, ZLF, and TZ conducted experiments, YY and LGL designed the experiments and wrote the paper, and LGL conceived the study. All the authors approved the final proof.

ADDITIONAL INFORMATION

Supplementary information The online version contains supplementary material available at https://doi.org/10.1038/s41401-021-00797-z.

Competing interests: The authors declare no competing interests.

REFERENCES

1. Ellulu MS, Patimah I, Khaza'ai H, Rahmat A, Abed Y. Obesity and inflammation: the linking mechanism and the complications. Arch Med Sci. 2017;4:851–63.

2. Lee CH. Young eosinophils rejuvenate ageing adipose tissues. Nat Metab. 2020;2:655–6.
3. Swanson KV, Deng M, Ting JP. The NLRP3 inflammasome: molecular activation and regulation to therapeutics. Nat Rev Immunol. 2019;19:477–89.
4. Li D, Liu Q, Sun W, Chen X, Wang Y, Sun Y, et al. 1,3,6,7-Tetrahydroxy-8-prenylxanthone ameliorates inflammatory responses resulting from the paracrine interaction of adipocytes and macrophages. Br J Pharmacol. 2018;175:1590–606.
5. Zhang T, Fang Z, Linghu KG, Liu J, Gan L, Lin L. Small molecule-driven SIRT3-autophagy-mediated NLRP3 inflammasome inhibition ameliorates inflammatory crosstalk between macrophages and adipocytes. Br J Pharmacol. 2020;177:4645–65.
6. Lee YS, Li P, Huh JY, Hwang IJ, Lu M, Kim JI, et al. Inflammation is necessary for long-term but not short-term high-fat diet-induced insulin resistance. Diabetes. 2011;60:2474–83.
7. Gao D, Madi M, Ding C, Fok M, Steele T, Ford C, et al. Interleukin-1β mediates macrophage-induced impairment of insulin signaling in human primary adipocytes. Am J Physiol Endocrinol Metab. 2014;307:E289–E304.
8. Ehses JA, Lacraz G, Giroix MH, Schmidlin F, Coulaud J, Kassis N, et al. IL-1 antagonism reduces hyperglycemia and tissue inflammation in the type 2 diabetic GK rat. Proc Natl Acad Sci USA. 2009;106:13998–4003.
9. He M, Chiang HH, Luo H, Zheng Z, Qiao Q, Wang L, et al. An acetylation switch of the NLRP3 inflammasome regulates aging-associated chronic inflammation and insulin resistance. Cell Metab. 2020;31:580–91.
10. Purushotham A, Schug TT, Xu Q, Surapureddi S, Guo X, Li X. Hepatocyte-specific deletion of SIRT1 alters fatty acid metabolism and results in hepatic steatosis and inflammation. Cell Metab. 2009;9:327–38.
11. Fu C, Hao S, Xu X, Zhou J, Liu Z, Lu H, et al. Activation of SIRT1 ameliorates LPS-induced lung injury in mice via decreasing endothelial tight junction permeability. Acta Pharmacol Sin. 2019;40:630–41.
12. Committee of Chinese Materia Medicine. Chinese materia medicine. Shanghai, China: Science Press; 2007, p. 643.
13. Dong T, Li C, Wang X, Dian L, Zhang X, Li L, et al. Ainsliadimer A selectively inhibits IKKalpha/beta by covalently binding a conserved cysteine. Nat Commun. 2015;6:6522.
14. Ren YM, Zhou SZ, Zhang T, Qian M, Zhang R, Yao S, et al. Targeted isolation of two disesquiterpenoid macrocephadiolides A and B from *Ainsliaea macrocephala* using a molecular networking-based dereplication strategy. Org Chem Front. 2020;7:1481–9.
15. Wu ZJ, Xu XK, Zeng HW, Shen YH, Tian JM, Su J, et al. New sesquiterpenoids from *Ainsliaea macrocephala* and their nitric oxide inhibitory activity. Planta Med. 2011;77:1545–50.
16. Feng ZL, Zhang T, Liu JX, Chen XP, Gan LS, Ye Y, et al. New podolactones from the seeds of *Podocarpus nagi* and their anti-inflammatory effect. J Nat Med. 2018;72:882–9.
17. Liu Q, Li D, Wang A, Dong Z, Yin S, Zhang Q, et al. Nitric oxide inhibitory xanthones from the pericarps of *Garcinia mangostana*. Phytochemistry. 2016;131:115–23.
18. Lin L, Pang W, Chen K, Wang F, Gengler J, Sun Y, et al. Adipocyte expression of PU.1 transcription factor causes insulin resistance through upregulation of inflammatory cytokine gene expression and ROS production. Am J Physiol Endocrinol Metab. 2012;302:E1550–E1559.
19. Zhang T, Liu J, Tong Q, Lin L. SIRT3 acts as a positive autophagy regulator to promote lipid mobilization in adipocytes via activating AMPK. Int J Mol Sci. 2020;21:372.
20. Dai H, Case AW, Riera TV, Considine T, Lee JE, Hamuro Y, et al. Crystallographic structure of a small molecule SIRT1 activator-enzyme complex. Nat Commun. 2015;6:7645.
21. Maier JA, Martinez C, Kasavajhala K, Wickstrom L, Hauser KE, Simmerling C. ff14SB: Improving the accuracy of protein side chain and backbone parameters from ff99SB. J Chem Theory Comput. 2015;11:3696–713.
22. Wang JM, Wolf RM, Caldwell JW, Kollman PA, Case DA. Development and testing of a general amber force field. J Comput Chem. 2004;25:1157–74.
23. Da Silva AWS, Vranken WF. ACPYPE-Antechamber python parser interface. BMC Res Notes. 2012;5:1–8.
24. Jafari R, Almqvist H, Axelsson H, Ignatushchenko M, Lundbäck T, Nordlund P, et al. The cellular thermal shift assay for evaluating drug target interactions in cells. Nat Protoc. 2014;9:2100–22.
25. Li D, Yang C, Zhu JZ, Lopez E, Zhang T, Tong Q, et al. Berberine remodels adipose tissue to attenuate metabolic disorders by activating sirtuin 3. Acta Pharmacol Sin. 2021. https://doi.org/10.1038/s41401-021-00736-y.
26. Liu J, Li D, Zhang T, Tong Q, Ye RD, Lin L. SIRT3 protects hepatocytes from oxidative injury by enhancing ROS scavenging and mitochondrial integrity. Cell Death Dis. 2017;8:e3158.
27. Daina A, Michielin O, Zoete V. SwissADME: a free web tool to evaluate pharmacokinetics, drug-likeness and medicinal chemistry friendliness of small molecules. Sci Rep. 2017;7:42717.
28. Stinchcomb DM, Pranata J. Conformational and tautomeric equilibria of formohydroxamic acid in the gas phase and in aqueous solution. J Mol Struct. 1996;370:25–32.
29. Faustin B, Lartigue L, Bruey JM, Luciano F, Sergienko E, Bailly-Maitre B, et al. Reconstituted NALP1 inflammasome reveals two-step mechanism of caspase-1 activation. Mol Cell. 2007;25:713–24.
30. Gross O, Thomas CJ, Guarda G, Tschopp J. The inflammasome: an integrated view. Immunol Rev. 2011;243:136–51.
31. Xin JZ, Wu JM, Hu GM, Gu HJ, Feng YN, Wang SX, et al. alpha1-AR overactivation induces cardiac inflammation through NLRP3 inflammasome activation. Acta Pharmacol Sin. 2020;41:311–8.
32. Fu Y, Wang Y, Du L, Xu C, Cao J, Fan T, et al. Resveratrol inhibits ionising irradiation-induced inflammation in MSCs by activating SIRT1 and limiting NLRP-3 inflammasome activation. Int J Mol Sci. 2013;14:14105–18.
33. He Q, Li Z, Wang Y, Hou Y, Li L, Zhao J. Resveratrol alleviates cerebral ischemia/reperfusion injury in rats by inhibiting NLRP3 inflammasome activation through Sirt1-dependent autophagy induction. Int Immunopharmacol. 2017;50:208–15.
34. Volt H, García JA, Doerrier C, Díaz-Casado ME, Guerra-Librero A, López LC, et al. Same molecule but different expression: aging and sepsis trigger NLRP3 inflammasome activation, a target of melatonin. J Pineal Res. 2016;60:193–205.
35. Solomon JM, Pasupuleti R, Xu L, McDonagh T, Curtis R, DiStefano PS, et al. Inhibition of SIRT1 catalytic activity increases p53 acetylation but does not alter cell survival following DNA damage. Mol Cell Biol. 2006;26:28–38.
36. Weisberg SP, McCann D, Desai M, Rosenbaum M, Leibel RL, Ferrante AW Jr. Obesity is associated with macrophage accumulation in adipose tissue. J Clin Invest. 2003;112:1796–808.
37. Lin L, Lee JH, Buras ED, Yu K, Wang R, Smith CW, et al. Ghrelin receptor regulates adipose tissue inflammation in aging. Aging. 2016;8:178–91.
38. Suganami T, Nishida J, Ogawa Y. A paracrine loop between adipocytes and macrophages aggravates inflammatory changes-Role of free fatty acids and tumor necrosis factor alpha. Arterioscler Thromb Vasc Biol. 2005;25:2062–8.
39. Lumeng CN, Bodzin JL, Saltiel AR. Obesity induces a phenotypic switch in adipose tissue macrophage polarization. J Clin Invest. 2007;117:175–84.
40. Russo L, Lumeng CN. Properties and functions of adipose tissue macrophages in obesity. Immunology. 2018;155:407–17.
41. Xu H, Barnes GT, Yang Q, Tan G, Yang D, Chou CJ, et al. Chronic inflammation in fat plays a crucial role in the development of obesity-related insulin resistance. J Clin Invest. 2003;112:1821–30.
42. Li D, Zhang T, Lu J, Peng C, Lin L. Natural constituents from food sources as therapeutic agents for obesity and metabolic diseases targeting adipose tissue inflammation. Crit Rev Food Sci Nutr. 2021;12:1947–65.
43. Carty M, Kearney J, Shanahan KA, Hams E, Sugisawa R, Connolly D, et al. Cell survival and cytokine release after inflammasome activation is regulated by the Toll-IL-1R protein SARM. Immunity. 2019;50:1412–24.
44. Everett BM, Donath MY, Pradhan AD, Thuren T, Pais P, Nicolau JC, et al. Anti-inflammatory therapy with canakinumab for the prevention and management of diabetes. J Am Coll Cardiol. 2018;71:2392–401.
45. Bian ZM, Field MG, Elner SG, Kahlenberg JM, Elner VM. Distinct CD40L receptors mediate inflammasome activation and secretion of IL-1β and MCP-1 in cultured human retinal pigment epithelial cells. Exp Eye Res. 2018;170:29–39.
46. Chen J, Chen ZJ. PtdIns4P on dispersed trans-Golgi network mediates NLRP3 inflammasome activation. Nature. 2018;564:71–76.
47. Westermark P, Andersson A, Westermark GT. Islet amyloid polypeptide, islet amyloid, and diabetes mellitus. Physiol Rev. 2011;91:795–826.
48. Duewell P, Kono H, Rayner KJ, Sirois CM, Vladimer G, Bauernfeind FG, et al. NLRP3 inflammasomes are required for atherogenesis and activated by cholesterol crystals. Nature. 2010;464:1357–61.
49. Csak T, Ganz M, Pespisa J, Kodys K, Dolganiuc A, Szabo G. Fatty acid and endotoxin activate inflammasomes in mouse hepatocytes that release danger signals to stimulate immune cells. Hepatology. 2011;54:133–44.
50. Vandanmagsar B, Youm YH, Ravussin A, Galgani JE, Stadler K, Mynatt RL, et al. The NLRP3 inflammasome instigates obesity-induced inflammation and insulin resistance. Nat Med. 2011;17:179–88.
51. Martinon F, Pétrilli V, Mayor A, Tardivel A, Tschopp J. Gout-associated uric acid crystals activate the NALP3 inflammasome. Nature. 2006;440:237–41.
52. Salminen A, Ojala J, Suuronen T, Kaarniranta K, Kauppinen A. Amyloid-β oligomers set fire to inflammasomes and induce Alzheimer's pathology. J Cell Mol Med. 2008;12:2255–62.
53. Liu Q, Zuo R, Wang K, Nong FF, Fu YJ, Huang SW, et al. Oroxindin inhibits macrophage NLRP3 inflammasome activation in DSS-induced ulcerative colitis in mice via suppressing TXNIP-dependent NF-kappaB pathway. Acta Pharmacol Sin. 2020;41:771–81.

54. Kastner DL, Aksentijevich I, Goldbach-Mansky R. Autoinflammatory disease reloaded: a clinical perspective. Cell. 2010;140:784–90.
55. Matsushita T, Sasaki H, Takayama K, Ishida K, Matsumoto T, Kubo S, et al. The overexpression of SIRT1 inhibited osteoarthritic gene expression changes induced by interleukin-1β in human chondrocytes. J Orthop Res. 2013;31:531–7.
56. Lin QQ, Yan CF, Lin R, Zhang JY, Wang WR, Yang LN, et al. SIRT1 regulates TNF-α-induced expression of CD40 in 3T3-L1 adipocytes via NF-κB pathway. Cytokine. 2012;60:447–55.
57. Zhang R, Chen HZ, Liu JJ, Jia YY, Zhang ZQ, Yang RF, et al. SIRT1 suppresses activator protein-1 transcriptional activity and cyclooxygenase-2 expression in macrophages. J Biol Chem. 2010;285:7097–110.
58. Ponugoti B, Kim DH, Xiao Z, Smith Z, Miao J, Zang M, et al. SIRT1 deacetylates and inhibits SREBP-1C activity in regulation of hepatic lipid metabolism. J Biol Chem. 2010;285:33959–70.
59. Hou X, Rooklin D, Fang H, Zhang Y. Resveratrol serves as a protein-substrate interaction stabilizer in human SIRT1 activation. Sci Rep. 2016;6:38186.
60. Wang H, Kubica N, Ellisen LW, Jefferson LS, Kimball SR. Dexamethasone represses signaling through the mammalian target of rapamycin in muscle cells by enhancing expression of REDD1. J Biol Chem. 2006;281:39128–34.
61. Shen S, Liao Q, Liu J, Pan R, Lee SM, Lin L. Myricanol rescues dexamethasone-induced muscle dysfunction via a sirtuin 1-dependent mechanism. J Cachexia Sarcopenia Muscle. 2019;10:429–44.
62. Xie J, Zhang X, Zhang L. Negative regulation of inflammation by SIRT1. Pharm Res. 2013;67:60–67.
63. Lin J, Cai Q, Liang B, Wu L, Zhuang Y, He Y, et al. Berberine, a traditional Chinese medicine, reduces inflammation in adipose tissue, polarizes M2 macrophages, and increases energy expenditure in mice fed a high-fat diet. Med Sci Monit. 2019;25:87–97.
64. Wang B, Sun J, Shi YH, Le GW. Salvianolic acid B inhibits high-fat diet-induced inflammation by activating the Nrf2 pathway. J Food Sci. 2017;82:1953–60.
65. Chen YY, Yan Y, Zhao Z, Shi MJ, Zhang YB. Bofutsushosan ameliorates obesity in mice through modulating PGC-1 alpha expression in brown adipose tissues and inhibiting inflammation in white adipose tissues. Chin J Nat Med. 2016;14:449–56.
66. Bode H, Brendel E, Ahr G, Fuhr U, Harder S, Staib AH. Investigation of nifedipine absorption in different regions of the human gastrointestinal (GI) tract after simultaneous administration of ^{13}C- and ^{12}C-nifedipine. Eur J Clin Pharmacol. 1996;50:195–201.